ELSEVIER

Chemical Physics 217 (1997) 131–143

Chemical Physics

Femtosecond quantum dynamics of photoassociation reactions: the exciplex formation of mercury

P. Backhaus, B. Schmidt

Institut für Physikalische und Theoretische Chemie, WE 3, Freie Universität Berlin, Takustrasse 3, D-14195 Berlin, Germany

Received 7 November 1996

Abstract

A quantum dynamical wave packet description of photoassociation reactions induced by short laser pulses is developed including both vibrational/translational and rotational degrees of freedom. Various levels of approximation (perturbation approach, rotating wave approximation) are discussed. Simulations of the exciplex formation of mercury are performed and related to recent pump-probe experiments by Marvet and Dantus (Chem. Phys. Lett. 245 (1995) 393). It is shown that in these experiments photoassociation is only due to bound ← free transitions and does not proceed via bound ← bound transitions from a Van der Waals precursor. The calculated spectra show both vibrational and rotational coherence structure which can be interpreted in terms of quantum beats between different rovibrational states populated during the photoassociation process. The thermally averaged spectra show good qualitative agreement with the experimental data. © 1997 Elsevier Science B.V.

1. Introduction

The breaking of existing bonds and the formation of new bonds are among the most elementary chemical reactions. In recent years, this field has been growing extremely rapidly because it especially benefitted from the advent of novel time-dependent methods both in experiment and in theory [1–3]. Due to the development of new spectroscopic techniques, the breaking and remaking of bonds can now be investigated in real time and thus offers the possibility to interrogate the transition state [4]. Parallel to the development of femtochemistry experiments, new techniques have been devised to solve the time-dependent Schrödinger or Liouville–von Neumann equation which lead to a revival of time-dependent quantum mechanics [5]. However, up to now most of these approaches have been limited to unimolecular reactions. Typically, a first laser pulse (pump) breaks a bond and a second laser pulse (probe) is used to monitor the decay, recombination, or the forming of a new bond.

In contrast to that, the field of time-dependent studies of bimolecular reactions is considerably less developed which is mostly due to difficulties concerning the initial state and the time zero for the subsequent dynamics. Among the few prominent examples are approaches to the abstraction reactions

$$H + OCO \rightarrow HO + CO$$

$$Br + I_2 \rightarrow BrI + I,$$

where the radical is produced by photodissociation of HI or HBr, respectively, which is weakly bound to the other reagent. The use of Van der Waals precursors in these quasi-bimolecular reactions helps to define an initial state with restricted reagent geometry and

PII S0301-0104(97)00035-9

to define a time zero [6–9]. Another example of a bimolecular reaction is the control of the xenon–iodine reaction

$$Xe + I_2 \rightarrow XeI + I, \quad (1)$$

where the concept of wave-packet timing by means of pulsed lasers has been invoked [10].

In the present paper we want to study the process of photoassociation as a simple prototype of truly bimolecular reactions. Unlike the reversed process of photodissociation [11], light induced association has received very little attention yet. Photoassociation processes can be understood as half-collisions in which a pair of colliding atoms is bound by the interaction with the electromagnetic field of a laser inducing a bound $\leftarrow$ free transition [12]. This process is especially simple to realize when the collision partners are initially in their weakly bound electronic ground state and are then transferred to an excited state which exhibits a considerably stronger bound. Apart from studies on rare gas halides [13–15] this concept has been used in a series of recent studies of laser assisted collisions of ultracold alkali atoms where the excited state has a strong well and is predominantly determined by the long-range attraction (R^{-3}) between s- and p-state atoms [16–21]. Another prototype of photoassociation reactions is the excimer formation of certain metals in the second column of the periodic table [22]. However, none of the above-mentioned experimental studies is concerned with the real time detection of the ro-vibrational dynamics of the product molecules. A first theoretical concept for the use of a pump-probe scheme with pulsed lasers to monitor the vibrational wavepacket dynamics of a photoassociation reaction can be found in the work of Machholm et al. [23]. It is mentioned that also a strategy for photoassociation in the electronic ground state using infrared laser pulses has been proposed recently [24].

The first realization of a pump-probe experiment on association is the work on femtosecond photoassociation spectroscopy by Marvet and Dantus. They investigated the exciplex formation of Hg_2 by means of ultrashort laser pulses [25,26]. With a pump laser pulse, a collision pair of ground state mercury atoms is excited into an excimer state

$$Hg(6^1S_0) + Hg(6^1S_0) + h\nu \rightarrow Hg_2(D^3\Sigma_u^+). \quad (2)$$

Then a probe laser pulse is used to excite the molecule into a higher state giving rise to depletion of the fluorescence from the $D^3\Sigma_u^+$ state. In this way, the process of bond formation can be monitored in real time. The experimentally observed pump-probe signal essentially shows two main features. Following binding excitation by the pump laser pulse, there are fast oscillations with periods of the order of 300 fs which prevail for the whole length of the transients of 6 ps. They are caused by coherent vibrations of the newly formed bond and demonstrate that the spectral width associated with the laser pulse is large enough to coherently prepare several vibrational states and to create a spatially localized wave packet in the excited state. First calculations of the vibrational dynamics by the present authors approximately reproduced the structure of the pump-probe spectra and confirmed that the observed pump-probe signal is indeed due to bound $\leftarrow$ free transitions and cannot be explained by the presence of Van der Waals precursors [27]. Furthermore, the transients exhibit a rotational anisotropy which can be interpreted in terms of rotational coherences [28,29]. Initially, the nascent Hg_2 molecules are produced with a preferential orientation of the molecular axis along the polarization direction of the pump laser. However, this rotational coherence dephases with a decay time of 1.1 ps due to the presence of different angular momenta (impact parameters) of Hg_2 collision pairs.

In this paper, we simulate pump-probe spectra of photoassociation processes involving transitions between electronic states. This model accounts for both vibrational and rotational dynamics of stabilized collision pairs. In the following Section 2 a numerical treatment is applied and compared with an analytical approach based on time-dependent perturbation theory similar to that of Ref. [23]. In Section 3 we present results of our simulations of the Hg_2 exciplex formation using parameters of the experiment by Marvet and Dantus [25]. We first consider the case of a single pure quantum state. For this case, we investigate transition probabilities and excited state vibrational dynamics induced by the pump pulse (Section 3.1) before we show how the dynamics is reflected in pump-probe spectra (Section 3.2). In the following Section 3.3 we describe a procedure to obtain fully averaged spectra and compare our results for Hg_2 with the experimental spectra. Finally, Section 4 concludes our work and gives an outlook.

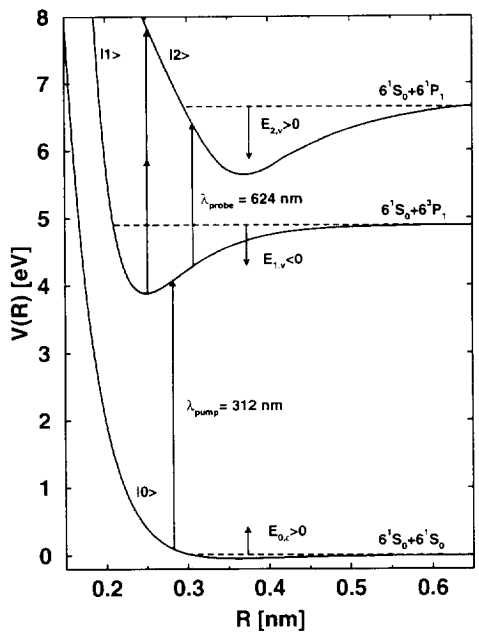

Fig. 1. Potential energy curves of the mercury molecule. The figure shows the three electronic states $|0\rangle$, $|1\rangle$, and $|2\rangle$ of our model together with the transitions corresponding to the wavelengths used in the pump-probe experiment of Ref. [25].

2. Methods

2.1. Model and potentials

Our model of the mercury dimer consists of three electronic states (see Fig. 1). In its electronic ground state XO_g^+ the two ground state Hg atoms (6^1S_0) are attracted by weak van der Waals forces only. The covalently bound first electronically excited state $D^3\Sigma_u^+$ is asymptotically connected to the mercury atoms in the 6^1S_0 and in the 6^3P_1 state. The second excited state considered here results from an avoided crossing of a $^1\Pi_g$ and a $^3\Sigma_g^+$ state [30] and correlates with Hg $6^1S_0 + 6^1P_1$. For simplicity, the three electronic states will be termed in the follwing $|0\rangle$, $|1\rangle$, and $|2\rangle$. The potential energy curves used in our simulations are based on experimental data. For the $|0\rangle$ and $|1\rangle$ states we assume Morse potentials with the spectroscopic constants adapted from Ref. [31] and a potential curve for the $|2\rangle$ state has been constructed from Fig. 4 of Ref. [32] (see Table 1).

In the framework of the Born–Oppenheimer approximation the total wave function of the Hg_2 system can

Table 1
Potential energy curves of Hg_2. The parameters ϵ, R_m, and β give the well depth, the equilibrium bond length, and the range parameter of the Morse potentials used in our simulations. The asymptotic energy E_i for the limit of separated atoms is given in the last column. ([a] For state $|2\rangle$ the potential curve is constructed from a spline fit to Fig. 4 of Ref. [32].)

$\|i\rangle$	state	ϵ [eV]	R_m [nm]	β [nm^{-1}]	E [eV]
$\|0\rangle$	XO_g^+	0.046	0.363	12.47	0
$\|1\rangle$	$D^3\Sigma_u^+$	1.004	0.250	17.27	4.888
$\|2\rangle$	$^1\Pi_g$ / $^3\Sigma_g^+$	1.063	0.370	–[a]	6.703

be written as

$$|\Psi(t)\rangle = \sum_{i=0}^{2} |i\rangle \otimes \left(\sum_{J=0}^{\infty} |\chi_{i,J}(t)\rangle \otimes |J\rangle \right), \qquad (3)$$

where $|i\rangle$ are electronic wave functions. The nuclear dynamics in the state corresponding to $|i\rangle$ is represented using the method of partial waves. A sum of products of radial ($|\chi_{i,J}(t)\rangle$) and angular ($|J\rangle$) functions describes vibrational and rotational dynamics, respectively. Note that a directional quantum number M is omitted here because we want to restrict ourselves only to pump-probe experiments with linearly polarized light and with parallel direction of excitation and detection ($M = 0, \Delta M = 0$). In this basis the Hamiltonian can be expressed as

$$\hat{H}(t) = \hat{H}_{mol} + \hat{W}(t), \qquad (4)$$

in which the time-independent molecular Hamiltonian is given by

$$\hat{H}_{mol} = \sum_i \left(\hat{T}_i + \hat{V}_{i,J} \right) |i\rangle\langle i|, \qquad (5)$$

with $\hat{T}_i$ being the operator for the radial part of the kinetic energy of the $^{202}Hg_2$ system and and $\hat{V}_{i,J}$ being the effective potential energy including the centrifugal barrier. The time-dependent part of the Hamiltonian (4) describes the interaction

$$\hat{W}(t) = -\sum_{i \neq j} \mathcal{E}(t) \cdot \hat{\boldsymbol{\mu}}_{j \leftarrow i} |j\rangle\langle i|, \qquad (6)$$

between the molecular transition dipole moment $\mu_{j \leftarrow i}$ and an external electric field $\mathcal{E}(t)$ in the semiclassical dipole approximation. For the $|1\rangle \leftarrow |0\rangle$ transition, we take the transition dipole moment function from

a spline interpolation to tabulated values in the literature [33]. For the $|2\rangle \leftarrow |1\rangle$ transition we assume a constant dipole moment of 2.54 D because reliable data are not available.

The laser pulses are of the form

$$\mathcal{E}(t) = \mathcal{E}_p g_p(t) \cos(\omega_p t), \tag{7}$$

where $\mathcal{E}_p$ and ω_p are the amplitude and the frequency of the pulse, respectively. The pulse shape is given by the function (see Ref. [34])

$$g_p(t) = \sin^2(\pi t/\tau_p), \quad 0 \le t \le \tau_p, \tag{8}$$

with a pulse duration $\tau_p = 2T_p$ which is very similar to a Gaussian pulse shape with a FWHM of T_p but offers the advantage of a well defined beginning and end of the pulse. The parameters are taken from the experimental work by Marvet and Dantus [25]. The probe pulse which is used to induce the $|2\rangle \leftarrow |1\rangle$ transition has an amplitude of 88.5 MV/cm and a wavelength of 624 nm. The pump pulse is frequency-doubled (312 nm) and its amplitude is reduced by a factor of ten (8.85 MV/cm). Both pulses have a full width at half maximum of $T_p = 65$ fs.

2.2. Numerical treatment of the model

In the following we repesent the nuclear wavefunctions of the Hg_2 system in a basis of vibrational $|v_{i,J}\rangle$ and free continuum states $|\epsilon_{i,J}\rangle$.

$$\begin{aligned}|\chi_{i,J}(t)\rangle = &\sum_v c_{i,v,J}(t) \exp[-i(E_i + E_{i,v,J})t/\hbar]|v_{i,J}\rangle \\ &+ \int_{\epsilon>0} d\epsilon\, c_{i,\epsilon,J}(t) \exp[-i(E_i + E_{i,\epsilon,J})t/\hbar] \\ &\times|\epsilon_{i,J}\rangle,\end{aligned} \tag{9}$$

with time dependent coefficients $c_{i,v,J}(t)$ and $c_{i,\epsilon,J}(t)$, respectively. The vibrational and translational energies $E_{i,v,J}$ and $E_{i,\epsilon,J}$ are given with respect to the asymptotic energies E_i of the separated atoms corresponding to the electronic states $|i\rangle$.

Because the pump and probe laser pulses are not overlapping in time and because we are dealing with rather weak fields it is sufficient to consider a two-level system for a given time t. For the coupling of the states $|0\rangle$ and $|1\rangle$ by the pump laser pulse (and similarly for the coupling of $|1\rangle$ and $|2\rangle$ by the probe laser pulse) inserting the ansatz (9) into the time-dependent Schrödinger equation yields coupled differential equations for the coefficients. For example, the bound states dynamics in the first electronically excited state is obtained by left-multiplying with $\langle J| \otimes \langle v| \otimes \langle 1|$

$$\begin{aligned}&i\hbar(\partial/\partial t)c_{1,v,J}(t) \\ &= \sum_{v'}\sum_{J'} c_{0,v',J'}(t)\langle 1, v, J|\hat{W}(t)|0, v', J'\rangle \\ &\quad\times \exp[i(E_{1\leftarrow 0} + E_{1,v,J} - E_{0,v',J'})t/\hbar] \\ &\quad+ \int_{\epsilon>0} d\epsilon \sum_{J'} c_{0,\epsilon,J'}(t)\langle 1, v, J|\hat{W}(t)|0, \epsilon, J'\rangle \\ &\quad\times \exp[i(E_{1\leftarrow 0} + E_{1,v,J} - E_{0,\epsilon,J'})t/\hbar],\end{aligned} \tag{10}$$

where $E_{1\leftarrow 0}/\hbar$ is the frequency of the $6^3P_1 \leftarrow 6^1S_0$ transition of free mercury atoms. Expressions analogous to Eq. (10) for the coefficients $c_{1,\epsilon,J}(t)$ of the continuum part of the excited state wave function can be obtained by replacing v with ϵ. Similar equations for the dynamics of the electronic ground state $|0\rangle$ are obtained by interchanging the indices 0 with 1 throughout. In the present spin-less model, we restrict ourselves to transitions with $\Delta J = \pm 1$.

An analytical solution of the coupled integro-differential equations (10) is impossible because it involves matrix elements of the dipole moment operator between (bound or free) eigenfunctions of Morse oscillators corresponding to different electronic states. It is noted here that for infrared photodissociation involving only one electronic state an analytical solution is possible for the special case of $J = 0$ and for special forms of the transition dipole moment function [35–37]. Instead, the time-dependent Schrödinger equation is solved here numerically based on a grid representation. The radial nuclear wave functions are given on an equidistant grid in coordinate space using FFT techniques for the evaluation of the kinetic energy operator [38,39]. The grid consisting of 1024 equally spaced points ranges from 0.1 to 1 nm. For the discretization in time, the split-operator scheme [40] is chosen which has been generalized for the case of coupled electronic surfaces [41]. The time step of 0.1 fs can be increased up to 1 fs by using the rotating-wave appoximation without notable loss of accuracy in the pump-probe spectra.

The Schrödinger equation then has to be solved subject to the initial condition that the initial state is a

pure bound or scattering state. Bound state wave functions are calculated using a Fourier-grid Hamiltonian method [42]. Scattering states have been obtained numerically using a Runge–Kutta method [43] and are truncated in the asymptotic region at ca. 1 nm and normalized with respect to the energy ϵ. All Franck–Condon factors and spectral intensities are given in arbitrary units.

2.3. Perturbation theory

The system of integro-differential equations given in Eq. (10) can be simplified substantially under certain assumptions which shall be discussed here in detail. First, time dependent perturbation theory to first order can be applied if the laser intensities are not extremely large and hence the coupling elements occuring in Eqs. (10) are very small [44,11]. Then the time-dependent coefficients $c_{0,v',J'}$ and $c_{0,\epsilon,J'}$ on the right hand side of the differential equations (10) can be replaced by their initial values, i. e. we assume the ground state wavefunction to be essentially unchanged by the pump pulse. As a consequence, the dynamics of the excited state $|1\rangle$ becomes uncoupled from the ground state dynamics. Additionally, we are assuming that the wavelength of the pump laser is chosen such that population of continuum states of $|1\rangle$ can be neglected. Starting from the initial conditions given above, for the example of a initial state of a free partial wave with energy ϵ and angular momentum J only one system of uncoupled equations has to be solved [23]

$$i\hbar\frac{\partial}{\partial t}c_{1,v,J}(t) = \sum_{J'} c_{0,\epsilon,J'}\langle 1, v, J|\hat{W}(t)|0, \epsilon, J'\rangle. \tag{11}$$

Inserting the analytical form (7) for the time-dependence of the electric field and using the rotating-wave approximation yields

$$c_{1,v,J}(\tau_p) = -\frac{\mathcal{E}_p}{2i\hbar}\sum_{J'}\langle J|\cos\theta|J'\rangle\langle 1, v, J|\mu_{1\leftarrow 0}|0, \epsilon, J'\rangle \times \int_{t=0}^{2\tau_p} dt\, g_p(t)\exp(i\Omega_{1,v,J\leftarrow 0,\epsilon,J'}t), \tag{12}$$

where the detuning Ω is defined as the difference between the frequency of the laser pulse and the resonant transition frequency of the levels $(0, \epsilon, J')$ and $(1, v, J)$

$$\Omega_{1,v,J\leftarrow 0,\epsilon,J'} = (E_{1\leftarrow 0} + E_{1,v,J} - E_{0,\epsilon,J'})/\hbar - \omega_p. \tag{13}$$

The matrix elements of the direction cosine between the laser polarisation (along z-axis) and the transition dipole moment $\mu_{1\leftarrow 0}$ for $J' = J \pm 1$ are given by [45]

$$\langle J|\cos\theta|J+1\rangle = (J+1)[(2J+1)(2J+3)]^{-1/2}$$
$$\langle J|\cos\theta|J-1\rangle = J[(2J-1)(2J+1)]^{-1/2}. \tag{14}$$

For certain types of time-dependent fields, Eq. (12) can be integrated analytically. Apart from the case of a plane wave ($g_p(t) = 1$) [44] and the case of a Gaussian-shaped pulse [11], Eq. (12) can also be integrated directly for the $\sin^2$-shaped pulse of Eq. (8)

$$\int_{t=0}^{\tau_p} dt\, \sin^2(\pi t/\tau_p)\exp(i\Omega t) = \frac{i[\exp(iX) - 1]}{2\Omega[(X/2\pi)^2 - 1]}, \tag{15}$$

giving an effective line shape function for the laser pulse with $X = \Omega T_p$. It is noted that the coefficients are constant after the end of the pump laser pulse and before the beginning of the probe laser pulse. Hence, the time evolution in the electronically excited state $|1\rangle$ is completely determined by the phase factors of the natural time evolution of the bound states as shown in the first term of the right hand side of Eq. (9).

3. Results

3.1. Vibrational wave packet dynamics

First, we want to discuss excitation probabilities induced by the pump laser pulse. We consider probabilities $|c_{1,v,J}|^2$ from a continuum state of the colliding ground state Hg atoms with given translational energy ϵ and given angular momentum J to a certain rovibrational level $|1, v, J\rangle$ of the first electronically excited state at the end of the laser pulse ($t = \tau_p$). In

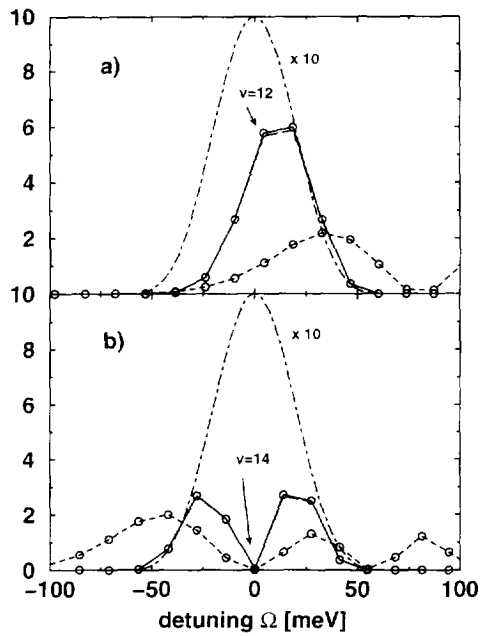

Fig. 2. Association probabilities in arbitrary units $|c_{1,v,J}(\tau_p)|^2$ at the end of the pump laser pulse for two different collision energies. (a) $\epsilon = 93$ meV ($J = 0$). (b) $\epsilon = 125$ meV ($J = 0$). The solid line shows the exact results of Eq. (16) while the long-dashed line gives the results of Eq. (12) obtained from perturbation apprach. Also given are the Franck–Condon factors $|\langle 1, v, J|\mu_{1\leftarrow 0}|0, \epsilon, J\rangle|^2$ as short-dashed line and the effective line shape of the laser pulse of Eq. (15) as dot-dashed curve.

the numerical calculations using grid methods, association probabilities can be obtained by projecting the (energy-normalized) wave function at the end of the pump laser pulse on the bound state functions v of the excited state $|1\rangle$

$$c_{1,v,J}(\tau_p) = \langle v_{1,J}|\chi_{1,J}(\tau_p)\rangle. \tag{16}$$

This has to be compared with the perturbation approach as described above, for which these coefficients are given in Eq. (12). Fig. 2 shows our results for the two methods. It can be seen that the differences between the two methods are extremely small. Throughout the interval $0 < \epsilon \leq 1$ eV they never exceed 1 %. Hence, for the laser intensities considered here, the use of the perturbation ansatz is fully justified. The average speed-up of the calculations is of the order of 50.

Furthermore, the formulation in perturbation approach has another important advantage over the numerical grid method. It is evident that Eq. (12) allows an intuitive interpretation of the probability for photoassociation ($|c_{1,v,J}(\tau_p)|^2$) which are determined by two quantities. The first one is the square of the integral (15) which can be regarded as an effective line-shape function of the laser pulse which is centered around the resonance condition $\Omega = 0$ with a half width at full maximum of $\Delta = \Omega T_p \approx \pm 2.26$ [23]. For the pulses considered here ($T_p = 65$ fs) this corresponds to excitation of vibrational states within an energy range of approximately $2\Delta\hbar/T_p \approx 90$ meV.

The second factor determining the transition probabilities is the Franck–Condon factor

$$|\langle 1, v, J|\mu_{1\leftarrow 0}|0, \epsilon, J \pm 1\rangle|^2,$$

of the respective transition [46]. According to a reflection principle, these factors are known to mimic the bound state wave function $|1, v, J\rangle$ [47]. Because the minimum position of the excited state $|1\rangle$ is shifted inwards with respect to the repulsive wall of the electronic ground state potential (see Fig. 1) the Franck–Condon factors are practically zero up to a certain quantum state $|1, v_{min}, J\rangle$. For a typical collision energy of $\epsilon_0 = 100$ meV, the first eight factors are vanishing. For higher energies, this threshold shifts to even larger v_{min}. Beyond this threshold, the oscillatory structure typical for bound←free transitions is observed.

This situation is depicted in Fig. 2 where the transition probabilities $|c_{1,v,J}(\tau_p)|^2$ are shown together with the Franck–Condon factors and the energy distribution of the laser pulse. For a scattering energy of $\epsilon = 93$ meV and s-wave scattering ($J = 0$), the spectral width of the laser pulse covers about four vibrational levels (see Fig. 2a). Hence, the excited state wave function created by the pump pulse essentially is a superposition of the vibrational eigenstates $v = 11, 12, 13, 14$. The initial time evolution of the vibrational wave functions is shown in Fig. 3a. The first pulse forms one well localized wave packet around an internuclear separation of 0.285 nm. Then the wave packet starts moving inwards and outwards periodically. A first order estimate for the vibrational period is the classical oscillation time

$$T_{osc} = \frac{h}{E_{v_1+1} - E_{v_1}}. \tag{17}$$

For a central vibrational level $v = 12$ this yields a period of $T_{osc} = 292$ fs. This illustrates why there is

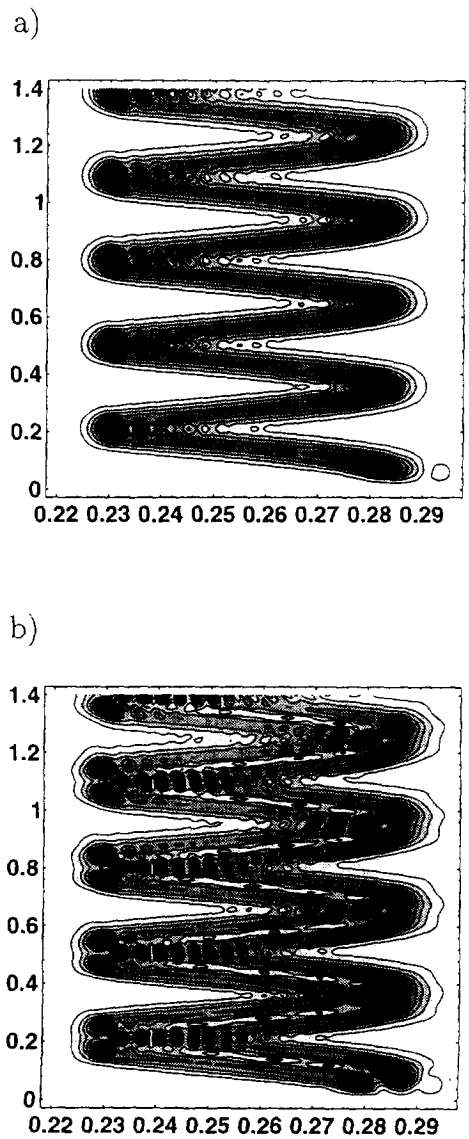

Fig. 3. Short time vibrational wave packet dynamics of Hg_2 in the excited state $|1\rangle$ for two different collision energies. (a) $\epsilon = 93$ meV ($J = 0$). (b) $\epsilon = 125$ meV ($J = 0$). The figure shows contours of the modulus of the wave packet $|\chi_{1,J}|$ as a function of the distance in nm (abscissa) and the time in ps (ordinate).

no strong spreading of the wave function during the pump process. The condition that the duration of the laser pulse is at most one third or one quarter of T_{osc} is equivalent to the requirement that the spectral width of the laser as given in Eq. (15) covers at least three to four vibrational levels [23].

Another situation arises for higher collision energies. It can be seen in Fig. 2b that for $\epsilon = 125$ meV the central energy of the laser pulse coincides with a minimum of the Franck–Condon factor at $v = 14$. This leads to a bimodal distribution of transition probabilities $|c_{1,v,J}(\tau_p)|^2$ with one lobe at $v = 11, 12, 13$ and another one at $v = 15, 16, 17$. Accordingly, the wave function created in the excited state consists of two wave packets each of which is a spatially localized superposition of essentially three bound states (see Fig. 3b). The two wave packets oscillate independently of each other at a slightly higher frequency with a period of $T_{osc} = 296$ fs for a central vibration of $v = 14$. In the vicinity of the turning points there are strong interferences arising when one packet is still moving inwards while the other one is already reflected. These interferences are stronger at the inner than at the outer turning point because of the steeper potential.

An essential feature of the vibrational dynamics in anharmonic systems is depicted in Fig. 4. After the first few periods of oscillation the wave packet starts to spread gradually which limits the classical-like behavior to the first few ps. This spreading, however, is not completely irreversible [48,49] . It can be shown that after a time period of

$$T_{rev} = \frac{2T_{osc}}{|\partial E_{1,v,J}/\partial E|}, \tag{18}$$

there is a so-called revival when the wave packet regains its original (spatially localized) form before it dephases again. Inserting the first order difference

$$E_{1,v+1,J} - E_{1,v,J} \approx E_{1,v,J}\,\partial E_{1,v,J}/\partial E, \tag{19}$$

yields a total revival time of 67.24 ps for a central vibrational state of $v = 12$ ($\epsilon = 93$ meV). Furthermore, it is known that for times near integer fractions of T_{rev} the wave packet is known to split into $n/2$ (for n even) or n (for n odd) spatially localized packets. This phenomenon is known as fractional revival [48,49]. In Fig. 4 the vibrational dynamics is shown for various time intervals. For times close to the total revival time $T \approx T_{rev}$ there is a localized wave packet centered around the classical path whose motion closely resembles that of the initial stage of the time evolution (see Fig. 3a). In the vicinity of the second order revival around $T \approx T_{rev}/2$ we have essentially the same picture but with a phase shift of π (see Fig. 4c). Around the time of the fourth order revival $T \approx T_{rev}/4$ there

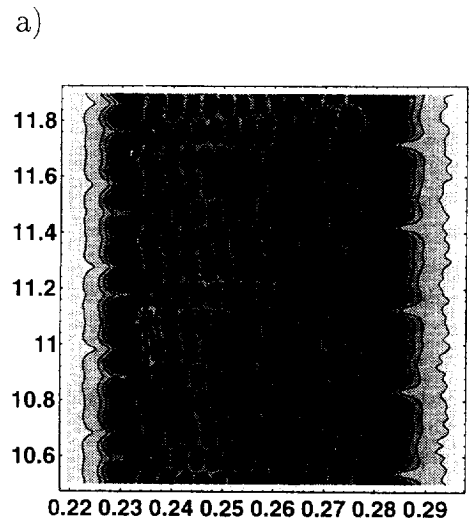

Fig. 4. Long time wave packet dynamics of Hg_2 in the state $|1\rangle$ for a collision energy of $\epsilon = 93$ meV ($J = 0$). The contour plots illustrate the evolution of $|\chi_{1,J}|$ within time windows of 1.4 ps centered around various fractions of the the total revival time. (a) $T_{rev}/6 = 11.21$ ps. (b) $T_{rev}/4 = 16.81$ ps. (c) $T_{rev}/2 = 33.62$ ps.

are two spatially localized wave packets both oscillating with a frequency of T_{osc} but with a phase shift of π with respect to each other (see Fig. 4b) giving rise to interference at the crossing points in the region of the potential well. Accordingly, there are three wave packets around the third order revival time $T \approx T_{rev}/6$ (see Fig. 4a).

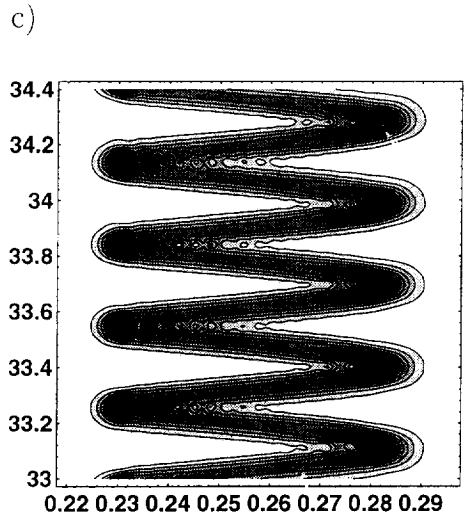

Fig. 4 — continued.

3.2. Pump-probe spectra

In the following we will discuss how the excited state vibrational dynamics is reflected in the transients obtained in pump–probe spectra. As suggested by the experimental work of Marvet and Dantus, the vibrational dynamics induced by the first laser pulse is monitored by fluorescence decay of state $|1\rangle$ to the ground state $|0\rangle$ which occurs on a nanosecond timescale [25]. After a certain time delay Δt a second laser pulse is used to excite the molecule to a higher state $|2\rangle$ for which spontaneous emission to the ground state is dipole-forbidden. Thus the probe pulse serves to deplete the fluorescence signal. In our calculations we simply take the norm of the wave function in the electronic state $|2\rangle$

$$I(\Delta t; \epsilon, J) = \langle \chi_{2,J} | \chi_{2,J} \rangle, \tag{20}$$

as a measure for the contribution of a particular partial wave to the depletion detected in the pump-probe experiments. The arguments ϵ and J denote the dependence of the intensity on the initial state which is assumed to be a single partial wave with angular momentum $J \pm 1$ and with well-defined scattering energy ϵ. Analogously, $I(\Delta t; v, J)$ is defined as the contribution from a bound rovibrational state.

Fig. 5 shows our results for the two collision energies considered above (93 meV and 125 meV). The

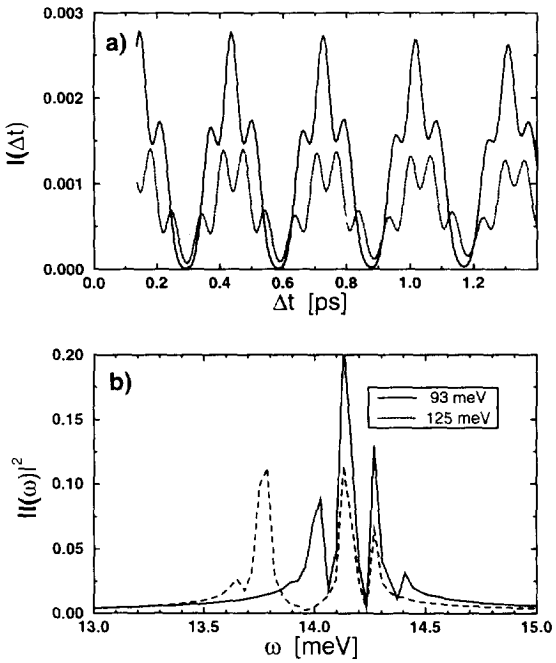

Fig. 5. Simulated pump-probe spectra (in arb. units) of the Hg_2 photoassociation for different collision energies (ϵ = 93 meV (solid curve) and ϵ = 125 meV (dashed curve)). The upper panel (a) shows the population $I(\Delta t)$ in state $|2\rangle$ as a function of the delay time Δt between the pump and the probe pulse. The lower part (b) gives the square of the Fourier transforms $|I(\omega)|^2$ of the transients.

simulated time-dependent transients of Fig. 5a exhibit periodic undulations with a period of 292 fs or 296 fs, respectively, corresponding to the classical oscillation periods mentioned above. It is observed that each of the maxima splits into three or four peaks, respectively. This splitting can be explained by considering the difference between the potential energy curves for state $|1\rangle$ and $|2\rangle$ in Fig. 1. It is evident that the transition induced by the probe pulse must be due to a two-photon absorption around r = 0.25 nm. One-photon processes can be ruled out since the suitable region around 0.31 nm is beyond the outer turning point of the vibrational dynamics in state $|1\rangle$ (see Fig. 3). Hence, the pump-probe signal can be regarded as a convolution of the time-dependent wavefunction at a distance of 0.25 nm with the time profile of the probe laser pulse. For example, it is evident from Fig. 3a that for ϵ = 93 meV the duration of the probe pulse (130 fs) can cover one ($\Delta t \approx$ 370 fs), two ($\Delta t \approx$ 435 fs), or again one ($\Delta t \approx$ 500 fs) lobe(s) of the wavefunction which explains the secondary maxima to both sides of the main maximum.

Another way to understand the simulated pump-probe signals is to analyse the pump-probe signals in frequency domain. For this purpose, we consider the square of the Fourier-transforms $|I(\omega)|^2$ of the transients as shown in Fig. 5b. The total length of our simulated transients of 140 ps corresponds to a frequency resolution of 0.03 meV. In the frequency domain, the main feature is a triple maximum around 14 meV which repeats at double and triple frequency. These signals can be interpreted in a straightforward manner. As has been mentioned before, the vibrational wave packet created in state $|1\rangle$ is a coherent superposition state comprising a few vibrational eigenstates having a well-defined phase relationship with respect to each other. Therefore, the signal in a pump-probe experiment can be phrased in terms of quantum beats between the individual states comprising the wave packet. The three peaks in the transient for ϵ = 93 meV at 14.02 meV, 14.14 meV and 14.26 meV are quantum beats between the states $v = 13/v = 14$, $v = 12/v = 13$, and $v = 11/v = 12$, respectively. Accordingly, for ϵ = 125 meV there are quantum beats between the states $v = 16/v = 17$ (13.65 meV) and $v = 15/v = 16$ (13.77 meV) corresponding to the one wave packet and beats between $v = 12/v = 13$ (14.14 meV) and $v = 11/v = 12$ (14.26 meV) for the other packet.

3.3. Averaged spectra

Up to now, we have considered only vibrational wave packet dynamics and pump-probe spectra $I(\Delta t; \epsilon, J)$ obtained for one pure initial state $(0, \epsilon, J)$ corresponding to a well-defined scattering energy ϵ and a specific partial wave J. Because it is not *a priori* clear whether the photoassociation reaction really starts from a collision pair (Hg + Hg) or from a preformed van der Waals molecule (Hg_2) we average over the contributions of all bound $(0, v, J)$ and free $(0, \epsilon, J)$ states to the pump-probe signal [15]

$$I(\Delta t; T) \propto f I_{\mathrm{bb}}(\Delta t; T) + (1 - f) I_{\mathrm{fb}}(\Delta t; T). \quad (21)$$

At a temperature of T = 433 K the ratio of the concentration of dimers versus monomers is only $f = 3.5 \times 10^{-5}$. For bound states, we simply have to sum over the contributions from all rovibrational states of Hg_2 with the correct statistical (Boltzmann) weights

$$I_{\mathrm{bb}}(\Delta t;T)=\sum_{v}\sum_{J}(2J+1)\mathrm{e}^{-E_{0,v,J}/kT}I(\Delta t;v,J). \tag{22}$$

For scattering states, realistic pump-probe spectra can be obtained from Eq. (20) in two steps. First, because the total nuclear wave function is represented as a sum over partial waves as indicated in Eq. (9), the contributions from individual partial waves have to be summed up for fixed scattering energy ϵ. Second, because the experiments are performed at a finite tempertature, the Maxwell–Boltzmann distribution of velocities has to be taken into account. Thus, the spectrum can be written as

$$I_{\mathrm{fb}}(\Delta t;T)=\int_{\epsilon}\mathrm{d}\epsilon\,\rho(\epsilon)\mathrm{e}^{-\epsilon/kT}\times\sum_{J}(2J+1)I(\Delta t;\epsilon,J), \tag{23}$$

where $\rho(\epsilon)$ is the density of states in the continuum ($\propto\sqrt{\epsilon}$) of dimension (energy)$^{-1}$.

We want to discuss the contribution of dimers versus that of collision pairs in Eq. (21). As mentioned above, the fraction f of mercury dimers is considerably smaller. Moreover, because of the limited range of the transition dipole moment function $\mu_{1\leftarrow 0}$, the pump-probe signal arising from a bound←bound transition ($I(\Delta t;v,J)$) is typically much smaller than that from a bound←free transition ($I(\Delta t;\epsilon,J)$). Hence, the first term on the right-hand side of Eq. (21) is neglected in the following.

Before discussing the averaged spectra we first want to consider the probability for the $1\leftarrow 0$ association induced by the pump laser pulse for different initial scattering states $(0,\epsilon,J)$. This transition probability which is defined as

$$p(\epsilon,J)=\sum_{v}|c_{1,v,J}(\tau_{\mathrm{p}})|^2, \tag{24}$$

determines the contribution of each scattering energy ϵ and each partial wave J to the wave function in state $|1\rangle$ and thus to the averaged spectra. It can be seen in Fig. 6 that for each J there is only a limited range of energies for which the excitation probabilities of Eq. (24) are non-vanishing. Basically, the curves $p(\epsilon,J)$ for fixed J can be explained in terms of a reflection principle for bound←free transitions similar

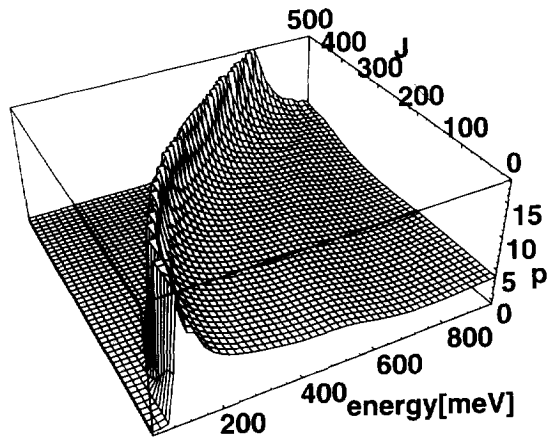

Fig. 6. Association probability in arb. units $p(\epsilon,J)$ at the end of the pump pulse as a function of the scattering energy ϵ and the angular momentum J of the initial free state.

to the reflection principle of photodissociation [47]. On the other hand, the association probability $p(\epsilon,J)$ for fixed scattering energy ϵ is determined by the position of the classical turning point of the scattering state relative to the Franck–Condon region for photoassociation. With increasing angular momentum J this point shifts towards larger distances and thus favors higher scattering energies. This trend, however, is limited by the Maxwell–Boltzmann distribution which is practically equal to zero for all scattering energies $\epsilon > 200$ meV. Therefore, the main contribution to the thermally averaged pump-probe signal of Eq. (24) originates from scattering energies in the range $0\leq\epsilon\leq 200$ meV and from angular momentum states with $0\leq J\leq 200$.

The resulting spectrum for a temperature of $T = 433$ K is shown in Fig. 7. As a consequence of the summation over various angular momenta J and the integration over ϵ, the vibrational structure is quite irregular compared to those shown in Fig. 5. However, the fundamental vibrational period of approximately 300 fs is still visible. This shows that the scenarios of Figs. 2 and 3 which were obtained for scattering energies in the range of $\epsilon\approx 100$ meV mainly determine the averaged spectra but the detailed structure, e. g. the formation of one or two wavepackets, are washed out.

Another interesting aspect of the averaged spectra is the rotational structure: Superimposed on the vibrational structure, there is a slow decay of the simulated

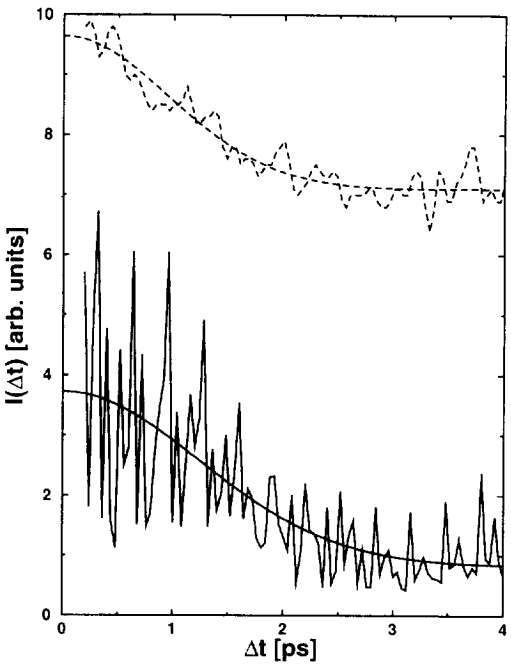

Fig. 7. Thermally averaged pump-probe spectra $I(\Delta t;T)$ for $T = 433$ K. For comparison, the experimental results obtained for parallel polarization are shown as dashed curve (see Ref. [25]). The smooth curves represent fits to the analytical form of Eq. (26) with $\tau_c = 1.75$ ps and $\tau_c = 1.33$ ps for the simulation and for the experiment, respectively.

pump-probe spectrum which can be explained in terms of rotational coherences [28,29]. The probe laser pulse can induce excitation to the rotational level J of the second electronically excited state $|2\rangle$ from both the levels $J-1$ and $J+1$ of the first excited state $|1\rangle$. Because of the different time evolution of these two states, the probe-signal is affected by quantum beats between them. Assuming the rotational level structure $E_J = BJ(J+1)$ of a diatomic molecule with a rotational constant of $B = 3.3$ μeV for $^{202}Hg_2$, the period of the rotational beats

$$T_{\mathrm{rot}} = \frac{h}{E_{J+1} - E_{J-1}} = \frac{h}{B(4J+2)}, \tag{25}$$

is typically found around $T_{\mathrm{rot}} = 3.11$ ps ($J = 100$). Averaging over the contributions of all partial waves of our ansatz (3) leads to rotational dephasing because of the J-dependence of T_{rot}. This gives rise to a decay as observed in our Fig. 7. Non-linear least-square fitting of our results to a Gaussian-like function

$$I(\Delta t;T) = A + B\,\exp[-(\Delta t/\tau_c)^2], \tag{26}$$

yields a dephasing time of $\tau_c = 1.75$ ps. This value is in satisfactory quantitative agreement with our fit to the experimental curve for parallel polarization of Ref. [25] where we obtain $\tau_c = 1.33$ ps.

4. Conclusions

In the first part of the present work a model for the theoretical treatment of pump-probe experiments on photoassociation reactions is developed (see Sections 2.1 and 2.2). The model consists of three electronic states and treats both bound and free scattering states. Based on the approach of Machholm et al. [23] our ansatz additionally includes the role of rotations. In Section 2.3 various approximations are considered. It is shown that for the experimental conditions considered here a perturbational approach and use of the rotating-wave approximation are fully justified and lead to considerable simplifications of the equations to be solved.

The model is applied to the process of exciplex formation of Hg_2. In our simulations we employ parameters corresponding to the femtosecond experiments by Marvet and Dantus where a pump laser pulse (312 nm) induces the $D^3\Sigma_u^+ \leftarrow XO_g^+$ photoassociation and a probe laser pulse (624 nm) further excites the molecule to deplete the fluorescence from the $D^3\Sigma_u^+$ state [25,26]. In agreement with the authors of those studies and our earlier results [27], we find that the photoassociation events observed in the experiments are indeed due to bound $\leftarrow$ free transitions, i. e. originate from free collision pairs (Hg + Hg), while the role of bound $\leftarrow$ bound transitions from preformed complexes (Hg_2) can be neglected. Thus we have shown that the femtosecond photoassociation spectroscopy is a truly bimolecular process not involving Van der Waals precursors (see Section 3.3). A comparison of measured and simulated pump-probe signals shows that the timescale for the decay of rotational coherence is in satisfactory quantitative agreement with the experiment where the faster decay in the experiment may be due to the abundance of several different isotopes in the sample. At present, the vibrational structure of experiment and simulation cannot be compared directly. Because the experimen-

tal transients are limited in length to 6 ps the corresponding resolution in the frequency domain is only 0.7 meV.

We want to emphasize the sensitivity of femtosecond photoassociation spectroscopy on the potential functions and dipole moment functions. It has been demonstrated in Section 3.1 that both the probability for photoassociation and the subsequent vibrational dynamics sensitively depend on the Franck–Condon factors for bound←free transitions and hence on the shape of the transition dipole moment (see Fig. 2). Moreover, Fourier transforms of the vibrational structure of the transients reveal the underlying quantum beats of the vibrational states comprising the wave packet created in the pump process. These beats are a direct measure for the vibrational level structure of Hg_2 in the $D^3\Sigma_u^+$ state (see Fig. 5b) and may serve to construct potential energy curves. Thus, the present femtosecond time-domain analysis of photoassociation of Hg atoms contains information equivalent to that obtained in frequency-domain spectroscopy with continous wave lasers. It remains to be seen whether femtosecond spectroscopy in atomic beam experiments can reach a similarly high resolution as obtained in conventional high-resolution spectroscopy of jet-cooled mercury [50].

Based on our present results, it is also possible to suggest modifications of the experiments of Refs. [25,26] and to make predictions. The present experiments involve photoassociation with the Hg_2 product in a superposition of ro-vibrational states $|1, v, J\rangle$ with v typically between 10 and 20 out of a total of 128 bound states. Possible modifications could be along two lines. By decreasing the detuning between the laser frequency ω_p and the $6^3P_1 \leftarrow 6^1S_0$ transition energy $E_{1\leftarrow 0}$ of isolated mercury atoms, the process of photoassociation would occur at larger internuclear separation. This would lead to excitation of considerably higher vibrational states. Due to the strong anharmonicity, a higher number of vibrational states could be excited with a laser of given effective line shape leading to better spatial localization of the wave packet but faster vibrational dephasing [23]. A contrary approach would be to optimize the pump laser pulses with the target to populate individual (ro-)vibrational levels. As suggested in previous work on photoassociation using pulsed infrared lasers [24], this could open new possibilities to produce state-selected molecules.

Acknowledgements

Financial support (grant Ma 515/14-1) by the Deutsche Forschungsgemeinschaft (DFG) through a program on "time-dependent phenomena in quantum systems of physics and chemistry" is acknowledged. Furthermore, the authors are grateful to Professor J. Manz for stimulating discussions and to Professor M. Dantus for making the experimental data of Refs. [25,26] available to us.

References

[1] A.H. Zewail, ed., Femtochemistry - Ultrafast Dynamics of the Chemical Bond (World Scientific, Singapore, 1994).
[2] J. Manz and L. Wöste, eds., Femtosecond Chemistry (Verlag Chemie, Weinheim, 1995).
[3] M. Chergui, ed., Ultrafast Chemical and Physical Processes in Molecular Systems (World Scientific, Singapore, 1996).
[4] A.H. Zewail, J. Phys. Chem. 100 (1996) 12701.
[5] K.C. Kulander, ed., Special Issue on Time-Dependent Methods For Quantum Dynamics, Comp. Phys. Commun., Vol. 63 (1991).
[6] N.F. Scherer, L.R. Khundkar, R.B. Bernstein and A.H. Zewail, J. Chem. Phys. 87 (1987) 1451.
[7] J.-P. Visticot, B. Soep and C.J. Whitham, J. Phys. Chem. 92 (1988) 4574.
[8] I.R. Sims, M. Gruebele, E.D. Potter and A.H. Zewail, J. Chem. Phys. 97 (1992) 4127.
[9] S.I. Ionov, G.A. Brucker, C. Jaques, L. Valachovic and C. Wittig, J. Chem. Phys. 99 (1993) 6553.
[10] E.D. Potter, J.L. Herek, S. Pedersen, Q. Liu and A.H. Zewail, Nature 355 (1992) 66.
[11] R. Schinke, Photodissociation Dynamics (Cambridge University Press, Cambridge, 1993).
[12] V.S. Dubov, L.I. Gudzenko, L.V. Gurvich and S.I. Iakovlenko, Chem. Phys. Lett. 45 (1977) 330.
[13] E.B. Gordon, V.G. Egorov, S.E. Nalivaiko, V.S. Pavlenko and O.S. Rzhevsky, Chem. Phys. Lett. 242 (1995) 75.
[14] J.H. Schloss, R.B. Jones and J.G. Eden, J. Chem. Phys. 99 (1993) 6483.
[15] G. Lo and D.W. Setser, J. Chem. Phys. 100 (1994) 5432.
[16] H.R. Thorsheim, J. Weiner and P.S. Julienne, Phys. Rev. Lett. 58 (1987) 2420.
[17] P.D. Lett, K. Helmerson, W.D. Phillips, L.P. Ratliff, S.L. Rolston and M.E. Wagshul, Phys. Rev. Lett. 71 (1993) 2200.
[18] L.P. Ratliff, M.E. Wagshul, P.D. Lett, S.L. Rolston and W.D. Phillips, J. Chem. Phys. 101 (1994) 2638.
[19] C.J. Williams and P.S. Julienne, J. Chem. Phys. 101 (1994) 2634.
[20] Y.B. Band and P.S. Julienne, Phys. Rev. A 51 (1995) 4317.
[21] P.D. Lett, P.S. Julienne and W.D. Phillips, Annu. Rev. Phys. Chem. 46 (1995) 423.
[22] G. Rodriguez and J.G. Eden, J. Chem. Phys. 95 (1991) 5539.

[23] M. Machholm, A. Giusti-Suzor and F.H. Mies, Phys. Rev. A 50 (1994) 5025.
[24] M.V. Korolkov, J. Manz, G.K. Paramonov and B. Schmidt, Chem. Phys. Lett. 260 (1996) 604.
[25] U. Marvet and M. Dantus, Chem. Phys. Lett. 245 (1995) 393.
[26] U. Marvet and M. Dantus, in: Ultrafast Chemical and Physical Processes in Molecular Systems, ed., M. Chergui (World Scientific, Singapore, 1996) pp. 138–142.
[27] P. Backhaus, J. Manz and B. Schmidt, in: Proceedings of the XXth Solvay Conference on Chemistry, Brussels, 28/11-2/12/95, to be published in Adv. Chem. Phys., 1996.
[28] S. Baskin, P.M. Felker and A.H. Zewail, J. Chem. Phys. 86 (1987) 2483.
[29] P.M. Felker and A.H. Zewail, J. Chem. Phys. 86 (1987) 2460.
[30] K. Balasubramanian, K.K. Das and D.W. Liao, Chem. Phys. Lett. 195 (1992) 487.
[31] J. Koperski, J.B. Atkinson and L. Krause, Chem. Phys. Lett. 219 (1994) 161.
[32] F.H. Mies, W.J. Stevens and M. Krauss, J. Mol. Spectr. 72 (1978) 303.
[33] E.W. Smith, R.E. Drullinger, M.M. Hessel and J. Cooper, J. Chem. Phys. 66 (1977) 5667.
[34] G.K. Paramonov and V.A. Savva, Phys. Lett. A 97 (1983) 340.
[35] T.M. Flosnik and R.E. Wyatt, Phys. Rev. A 40 (1989) 5716.
[36] M.V. Korolkov, Y.A. Logvin and G.K. Paramonov, J. Phys. Chem. 100 (1996) 8070.
[37] M.V. Korolkov, G.K. Paramonov and B. Schmidt, J. Chem. Phys. 105 (1996) 1862.
[38] R. Kosloff, J. Phys. Chem. 92 (1988) 2087.
[39] R. Kosloff, Annu. Rev. Phys. Chem. 45 (1994) 145.
[40] M.D. Feit, J.A. Fleck, Jr and A. Steiger, J. Comput. Phys. 47 (1982) 412.
[41] J. Alvarellos and H. Metiu, J. Chem. Phys. 88 (1988) 4957.
[42] C.C. Marston and G.G. Balint-Kurti, J. Chem. Phys. 91 (1989) 3571.
[43] W.H. Press, S.A. Teukolsky, W.T. Vetterling and B.P. Flannery, Numerical Recipes in Fortran (Cambridge University, Cambridge, 1992).
[44] R. Loudon, The Quantum Theory of Light (Clarendon, Oxford, 1973).
[45] A.R. Edmonds, Angular Momentum in Quantum Mechanics (Princeton University, Princeton, 1960).
[46] J. Tellinghuisen, Adv. Chem. Phys. 60 (1985) 399.
[47] G. Herzberg, Spectra of Diatomic Molecules (Van Nostrand-Reinhold, London, 1940).
[48] I.S. Averbukh and N.F. Perelman, Phys. Lett. A 139 (1989) 449.
[49] C. Leichtle, I.S. Averbukh and W.P. Schleich, Phys. Rev. Lett., to be published.
[50] R.D. van Zee, S.C. Blankespoor and T.S. Zwier, J. Chem. Phys. 88 (1988) 4650.